iScience, Volume *25*

Supplemental information

ACE2 can act as the secondary receptor in the FcγR-dependent ADE of SARS-CoV-2 infection

Zai Wang, Tingting Deng, Yulian Zhang, Wenquan Niu, Qiangqiang Nie, Shengnan Yang, Peipei Liu, Pengfei Pei, Long Chen, Haibo Li, and Bin Cao

Supplementary Figures

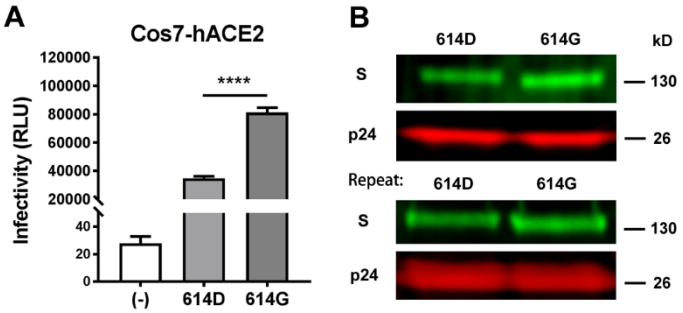

Figure S1. Generation of 614D and 614G pseudotyped viruses, related to Figure 1. (A) Infectivity of HIV/SARS-CoV-2 bearing S 614D (WT) or 614G on Cos7-hACE2 cells. Data were derived from three independent experiments, and are presented as mean±SD. One-way ANOVA was used to compare the difference between groups. ****p<0.0001. **(B)** SARS-CoV-2 S and HIV p24 proteins detected by Western blot.

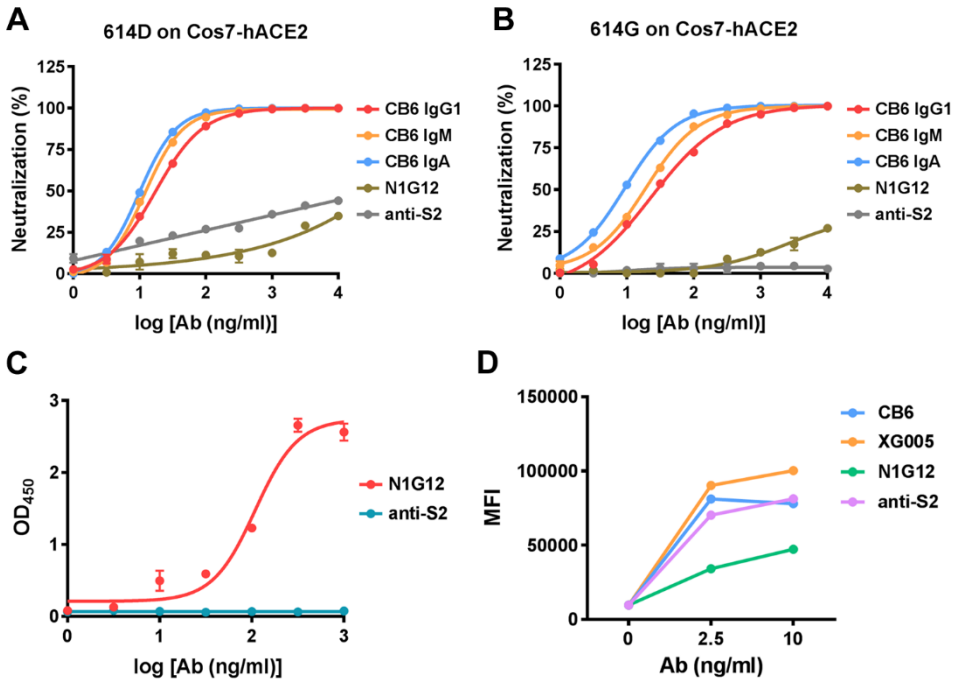

Figure S2. Neutralization ability of SARS-CoV-2 antibodies, related to Figure 1. (A and B) Neutralization ability of anti-S2, N1G12 and CB6 antibodies on 614D **(A)** and 614G **(B)** pseudovirus. **(C)** ELISA assay showing the binding abilities of N1G12 and anti-S2 to SARS-CoV-2 S1. Data were derived from three independent experiments, and are presented as mean±SD. **(D)** Flow cytometry assay showing the binding abilities of antibodies to S protein

expressed on 293T cells. Data were derived from assays in duplicates with mean values presented.

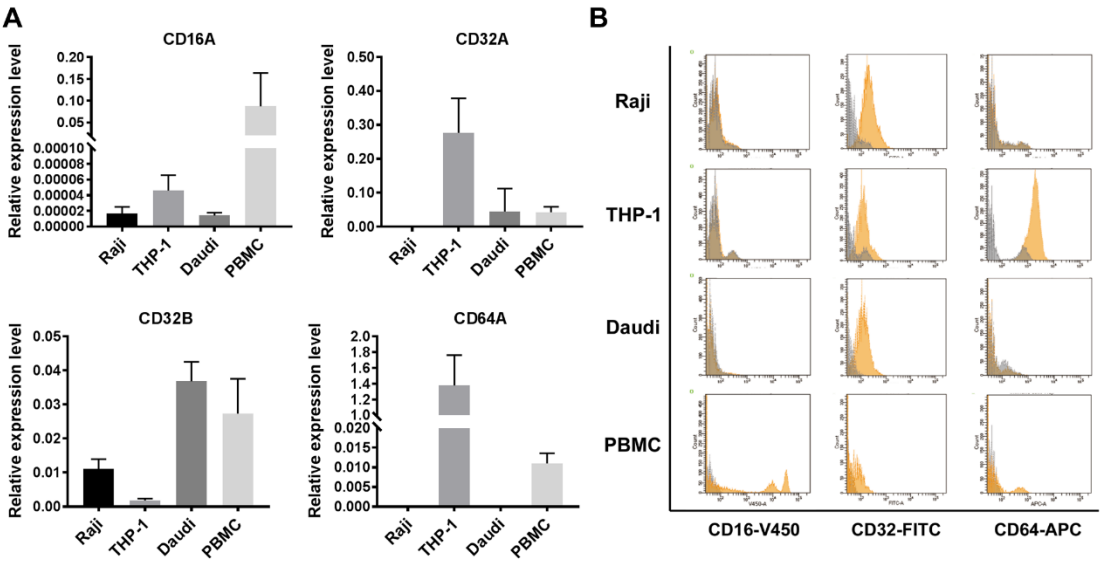

Figure S3. Surface expression of FcγRs on immune cells, related to Figure 1. (A) Real-time RT PCR was performed to analysis the mRNA level of CD16A, CD32A, CD32B and CD64A in THP-1, Raji, Daudi immune cell lines and PBMCs. Data were derived from three independent experiments, and are presented as mean±SD. **(B)** THP-1, Raji, Daudi and PBMCs were incubated with anti-CD16 conjugated with V450, anti-CD32 conjugated with FITC and anti-CD64 conjugated with APC, and then subjected to flow cytometry analysis. Non-targeting antibodies in IgG1 isotype conjugated with the same fluorophore were used as negative controls.

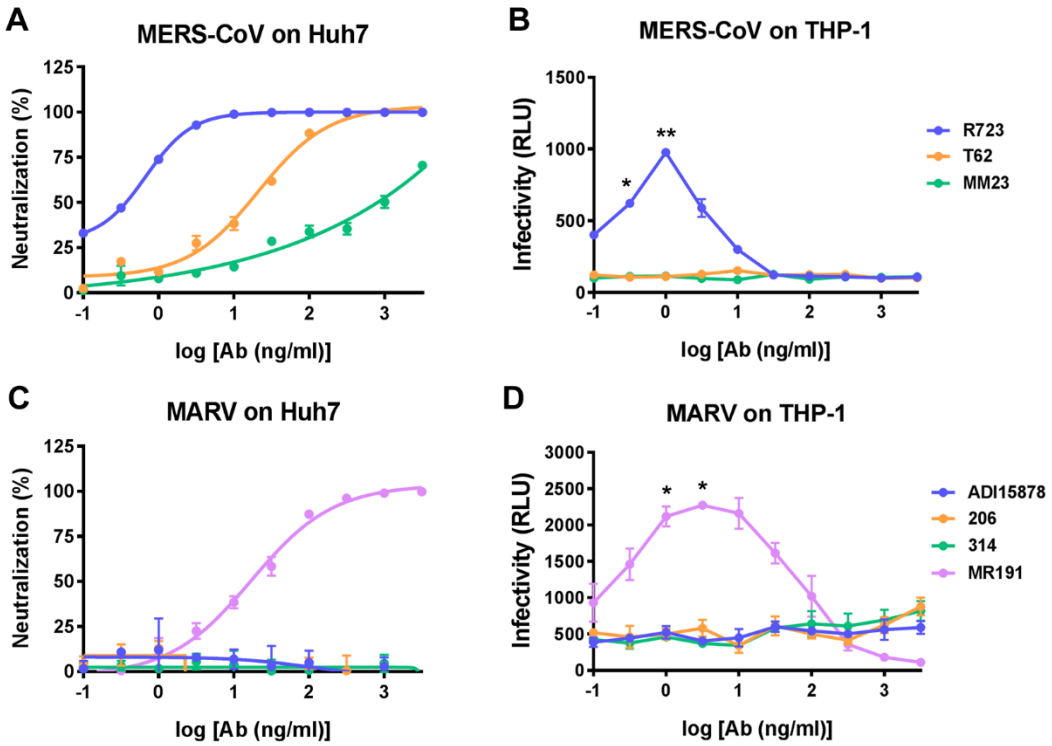

Figure S4. MERS-CoV and MARV exhibit ADE on THP-1 cells, related to Figure 1.

(A and B) Neutralization **(A)** and ADE **(B)** assays for HIV/MERS-CoV on Huh7 and THP-1 cells, respectively.

(C and D) Neutralization **(C)** and ADE **(D)** assays for HIV/MARV on Huh7 and THP-1 cells, respectively.

Data were derived from three independent experiments, and are presented as mean±SD. Repeated measurement of one-way ANOVA was used to compare the difference between the enhanced infectivity and the infectivity at basal level. *p<0.05; **p<0.01.

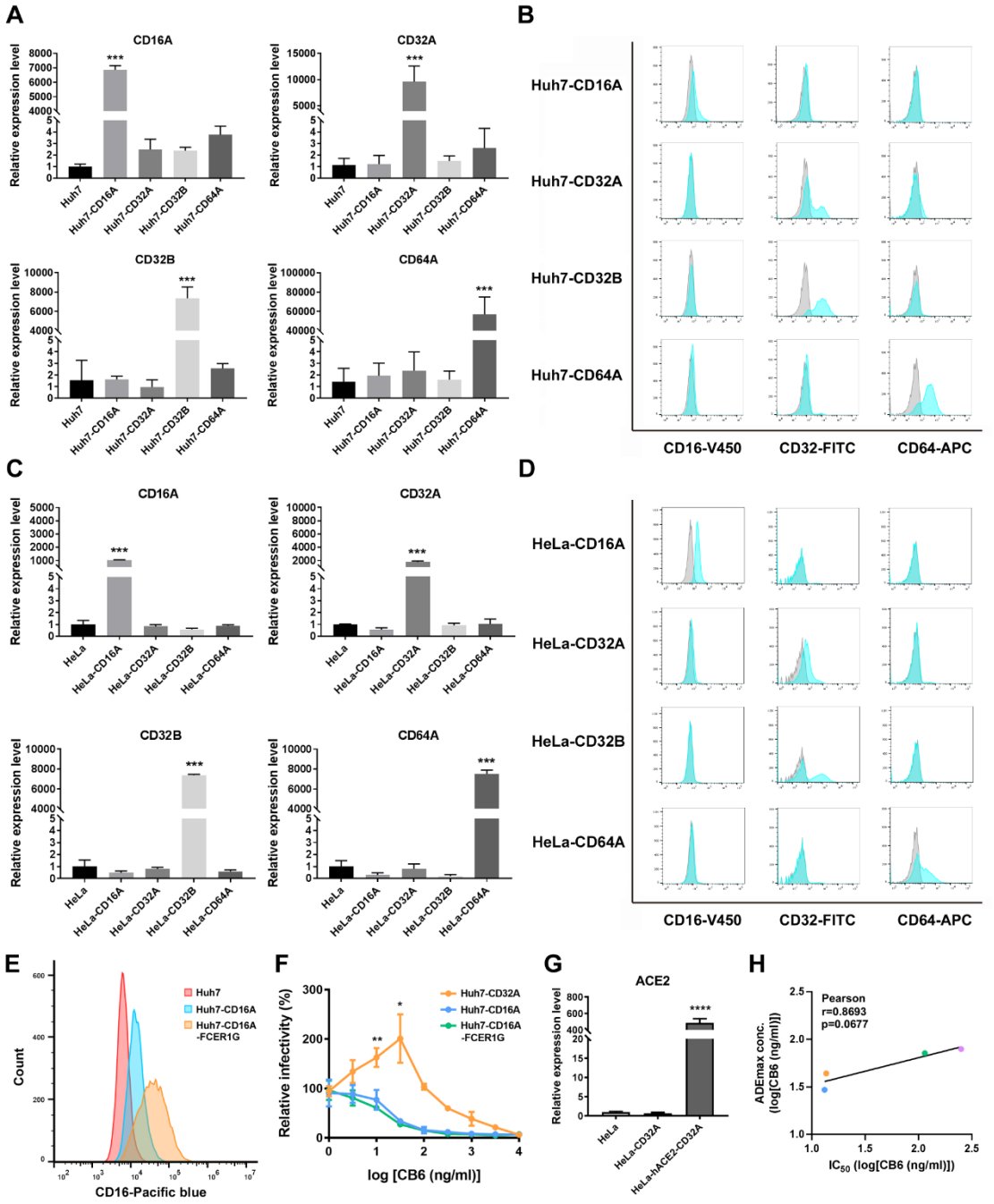

Figure S5. Establishment of FcγR-overexpressing cells, related to Figure 2. (A and C) Real-time RT PCR was performed to analysis the mRNA level of CD16A, CD32A, CD32B and CD64A in Huh7 **(A)** or HeLa **(C)** cells expressing different FcγRs. Data were derived from three independent experiments, and are presented as mean±SD. One-way ANOVA was used to compare the difference between control cell group (Huh7 or HeLa) and its derived cell group. ***p<0.001. **(B and D)** Huh7 **(B)** or HeLa **(D)** cells expressing different FcγRs were incubated with anti-CD16 conjugated with V450, anti-CD32 conjugated with FITC and anti-CD64

conjugated with APC, and then subjected to flow cytometry analysis. Huh7 **(B)** or HeLa **(D)** cells stained with the same antibodies were used as negative controls. ***p<0.001. **(E)** Cell surface expression of CD16A was improved with co-expression of FCER1G. Huh7, Huh7-CD16A and Huh7-CD16A-FCER1G cells were incubated with anti-CD16 conjugated with Pacific blue, and then subjected to flow cytometry analysis. **(F)** Improved cell surface expression of CD16A did not support CB6-mediated ADE. Relative infectivity of SARS-CoV-2 pseudovirus (614G) on Huh7-CD32A, Huh7-CD16A and Huh7-CD16A-FCER1G cells in the presence of different concentrations of CB6 IgG1. Data were derived from three independent experiments, and are presented as mean±SD. Repeated measurement of one-way ANOVA was used to compare the difference between the enhanced infectivity and the infectivity at basal level. *p<0.05. **(G)** Realtime PCR was performed to analysis the mRNA level of ACE2 in HeLa-derived cells. Data were derived from three independent experiments, and are presented as mean±SD. One-way ANOVA was used to compare the difference between control cell group (HeLa) and its derived cell group. ****p<0.0001. **(H)** Correlation analysis of maximum ADE induction concentration with IC_{50} for different variants: 614D (blue), 614G (orange), N501Y-D614G (green), E484K-N501Y-D614G (purple).

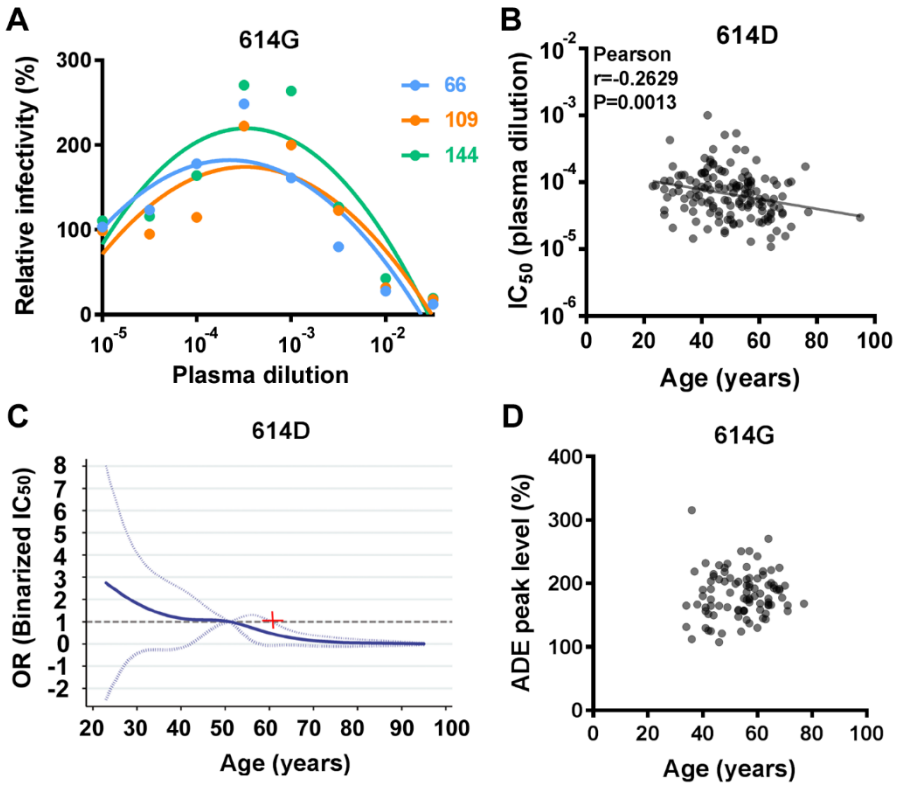

Figure S6. Analysis of neutralization and ADE characteristics of convalescent plasma, related to Figure 4 & Figure 5. (A) Representative data from 614G ADE assays using three convalescent plasma. a non-linear regression curve was fitted based on the relative infectivity values to derive the concentration of maximum induction of ADE. **(B)** Correlation of IC_{50} for 614D pseudovirus with patient age. A linear regression model was used for correlation analysis. **(C)** Cubic spline curve illustrating the prediction (in form of odds ratio or OR) for binarized IC_{50} of 614D variant with increasing age. The solid blue line represents the OR values, and the dotted light-blue lines represent the corresponding 95% confidence intervals. **(D)** No correlation was present between 614G ADE peak level and the patient age.

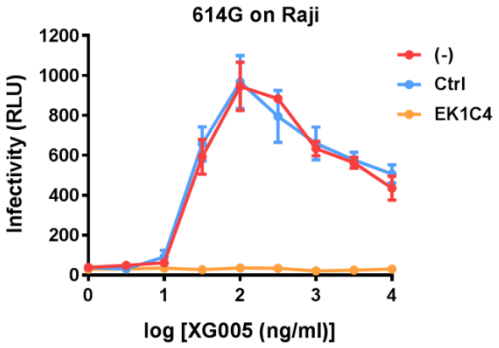

Figure S7. Membrane fusion is essential for XG005-mediated ADE on Raji cells, related to Figure 6.

Effect of EK1C4 on XG005-mediated SARS-CoV-2 (614G) ADE on Raji cells.

Data were derived from three independent experiments, and are presented as mean±SD.